JMEPEG (2021) 30:2691–2707
https://doi.org/10.1007/s11665-021-05662-y

1059-9495/$19.00

On the Interaction between Uniaxial Stress Loading and the Corrosion Behavior of the ISO 5832-1 Surgical Stainless Steel

Regiane Cristina Ferreira dos Santos, William Naville, Nelson Batista de Lima, Isolda Costa, and Renato Altobelli Antunes

Submitted: 3 September 2020 / Revised: 12 February 2021 / Accepted: 16 February 2021 / Published online: 23 March 2021

The interaction between the uniaxial stress loading and the corrosion behavior of the surgical ISO 5832-1 stainless steel is addressed in the present work. Specimens were subject to uniaxial tensile and compressive stress at two different deformation levels (15 and 30%). The effect of the different loading modes and deformation levels on the residual stresses was investigated by x-ray diffraction. The composition of the passive films formed on each sample was assessed by x-ray photoelectron spectroscopy (XPS). The corrosion behavior was studied by electrochemical impedance spectroscopy and potentiodynamic polarization in phosphate-buffered solution at 37 °C. The semiconducting character of the passive films was determined by the Mott-Schottky approach. Our findings point to a positive effect of compressive loading on the corrosion resistance of the steel. The passive current density (i_{pass}) decreased for the strained samples, especially for that subject to 15% compressive deformation for which i_{pass} was 63% lower than for the as-received steel. The passive film formed at this condition presented strong Cr_2O_3 enrichment, according to XPS results. Moreover, the compressive stresses favored the formation of a passive film with fewer defects, decreasing the donors density. The results are discussed based on the correlation between residual stresses, passive film composition and its electronic properties.

Keywords Mott-Schottky, passive film composition, plastic deformation, residual stresses, surface chemistry, surgical stainless steel

1. Introduction

Cold work is recognized as a critical aspect of the electrochemical behavior of austenitic stainless steels (Ref 1, 2). It is reported that plastic deformation strongly affects the dissolution rate of several metallic alloys (Ref 3, 4). The passive film of stainless steels is modified by the applied stresses, giving rise to increasing pitting susceptibility as a result of multiplied defects such as dislocations, enhancing the surface reactivity and also on residual stresses arising from deformation steps during mechanical processing (Ref 5-7). In fact, Accharyya et al. (Ref 8) have shown that surface stresses are responsible for increasing the reactivity of deformed 304 stainless steel samples, promoting localized corrosion spots.

Regiane Cristina Ferreira dos Santos and **Renato Altobelli Antunes**, Centro de Engenharia, Modelagem e Ciências Sociais Aplicadas (CECS), Universidade Federal do ABC (UFABC), Santo André, SP 09210-580, Brazil; **William Naville**, Fundação Educacional Ignaciana – FEI, São Bernardo do Campo, SP, Brazil; and **Nelson Batista de Lima** and **Isolda Costa**, Centro de Ciência e Tecnologia de Materiais (CCTM) – Instituto de Pesquisas Energéticas e Nucleares (IPEN/CNEN-SP), São Paulo, SP, Brazil. Contact e-mail: renato.antunes@ufabc.edu.br.

Navarov et al. (Ref 9) studied the effect of tensile stress on the passive film breakdown and repassivation of the AISI 304 stainless steel. They observed that the tensile stresses decreased the electrochemical potential up to 200 mV. The potential decrease was associated with the areas of internal residual stresses that led to heterogeneous potential distribution in the passive film and accelerated dissolution rate. Notwithstanding, there is still an intense debate about the effect of cold deformation on the corrosion resistance of stainless steels. For instance, Jinlong and Luo (Ref 10) investigated the effect of pre-tensile stresses on the stability of the passive film formed on AISI 304 stainless steel. They focused their research on the sensitization behavior of deformed samples and how chromium depleted regions were formed depending on the deformation level to which the stainless steel samples were subjected. The main findings of the experimental investigation were centered in the existence of a critical deformation level of only 10% for the tensile stress leading to increased corrosion susceptibility. From 20% up to 40% of deformation, there was a decrease of the degree of sensitization that was ascribed to an increase of chromium diffusivity, leading to desensitization when the deformed samples were heat-treated at an annealing temperature of 575 °C for 5 h. The critical chloride concentration for passive film rupture was found to decrease with the tensile stress level by Yang and Luo (Ref 11). It is reported that chromium diffusion is enhanced by the cold work of austenitic stainless steels, making the passive film less stable in chloride-containing solutions due to facilitated sensitization (Ref 12). Feng et al. (Ref 13) have shown that the composition of the passive film on the AISI 304 was modified by different deformation levels, especially with respect to oxidized iron species. Moreover, the doping density in the passive film was also dependent on the deformation level, increasing with the

strain percentage, thus rendering the oxide film more defective, conductive and prone to corrosion.

Surgical stainless steels have also been the target of several studies devoted to scrutinizing the role of cold work on the corrosion resistance and its correlation with passive film composition and semiconducting character. For instance, Ramírez et al. (Ref 14, 15) have reported an increase of the pitting corrosion susceptibility of the ISO 5832-1 stainless steel subjected to thickness reductions of up to 70% by cold rolling. The density of point defects in the passive film was associated with the observed pitting corrosion behavior in phosphate-buffered solution at 37 °C. Similarly, Jinlong et al. (Ref 16) have shown that the doping density in the passive film of a 316L-type surgical stainless steel was affected by prior deformation produced by tensile tests, giving rise to a more defective oxide film which was more prone to corrosion deterioration in a borate buffer solution. Talha et al. (Ref 17), in turn, reported increase in the corrosion resistance of a high-nitrogen surgical austenitic stainless steel in Hanks' solution at 37 °C after 20% cold work with respect to the pristine sample (0% cold work). Based on the findings of other authors (Ref 18-20), they hypothesized that the chromium content of the passive film was enhanced by cold work, improving the corrosion resistance.

Residual stresses are of utmost importance to the corrosion behavior of austenitic stainless steels (Ref 21, 22). It is well-propelled that several manufacturing processes generate surface stress levels that cannot be neglected if one considers corrosion failures of engineering alloys such as stress corrosion cracking or fatigue corrosion (Ref 23-25). According to Takakuwa and Soyama (Ref 26), compressive stresses are likely to improve the corrosion resistance of stainless steels whereas tensile residual stresses are often related to facilitated crack nucleation and growth, contributing to decreased reliability of structural components.

In one hand, individual aspects of passive film composition, residual stresses, cold work and the corrosion resistance of surgical stainless steels can be found in the current literature (Ref 27-29). Nonetheless, the interplay between all these aspects and also the semiconducting properties of the passive film is not deeply explored. For instance, some authors study the correlation between cold work, passive film composition and corrosion resistance but do not measure the surface residual stresses (Ref 12, 13, 19, 27, 28). Other reports focus on the correlation between residual stresses or cold work and the electrochemical behavior of stainless steels, but do not evaluate the passive film composition or its electronic properties (Ref 2, 5, 9, 10, 22-24, 26). Yet, if one considers biomedical stainless steels, study of such correlation is even scarcer. Few examples of specific information are found in (Ref 14-17). However, the correlation between residual stresses, passive film composition, corrosion behavior and semiconducting properties of the passive film is not studied.

In this scenario, the main contribution of the present work is to fill this gap by investigating the effect of different tensile and compressive uniaxial stress levels on the passive film composition, density of point defects, residual stresses and corrosion resistance of the ISO 5832-1 surgical stainless steel. Understanding of this complex interaction can drive the development of optimized surgical stainless steels by controlling the stress levels during stress-based manufacturing steps of implantable devices. This work is an initial step toward this important research field.

2. Materials and Methods

2.1 Material and Sample Preparation

The material used in this work was the ISO 5832-1 austenitic stainless steel (ASS) provided as 15.87 mm diameter bars in the solution-treatment condition by Villares Metals, Brazil. Pre-strained specimens were obtained after uniaxial tensile and compressive tests. The specimens for the mechanical tests were machined from the original bar, based on the ASTM E-8 and ASTM E-9 recommendations for the tensile and compressive tests, respectively.

Engineering strain levels were defined as 15 and 30% for both tensile and compressive specimens, controlled by longitudinal and transverse strain gages. The tests were conducted at room temperature in an MTS 810 machine at a crosshead speed of 10 mm min^{-1}. The as-received material was used as a reference for the 0% strain level.

Pre-strained specimens were obtained from the gauge length for the subsequent characterization techniques. The specimens (1 cm-length) were cut in a linear precision saw machine using diamond wafering blade and refrigeration with cutting fluid coolant. Then, the surface preparation was carried out by mechanical grinding with waterproof silicon carbide papers and polishing with diamond paste up to 1 μm.

2.2 Characterization

Residual stresses were measured by x-ray diffraction in a Rigaku DMAX Rint 2000 instrument operating with Cu-Kα radiation source (wavelength 0.154 nm). The measurements were made along the tangential direction with respect to the applied stresses during tensile and compressive tests. The stresses were determined based on the $\sin^2\psi$ method in the {1 1 1} crystallographic planes at $2\theta = 43°$. Microstructural characterization of the as-received and strained samples was carried out by confocal laser scanning microscopy (CLSM), using a Olympus, LEXT OLS4100 instrument. The samples were electrolytically etched in oxalic acid solution (10 wt.%) at a constant current density of 1 A cm^{-2} for 90 s, controlled by a D.C. power supply (Maisen MP3003D). A stainless steel plate was used as the cathode.

X-ray photoelectron spectroscopy (XPS) analysis was carried out in a Thermo VG K-alpha$^+$ spectrometer (Al-Kα, 1486.6 eV). The x-ray spot size was 400 μm. The pressure in the analysis chamber was approximately 10^{-7} Pa. High-resolution spectra were obtained in the $Fe2p_{3/2}$, $Cr2p_{3/2}$, Mo3d, $Ni2p_{3/2}$ and O1s regions. Peak fitting was carried out in the Avantage™ software using the Smart algorithm with a mixture of Lorentzian-Gaussian functions. The binding energy scale was calibrated with respect to the C1s peak (adventitious carbon) at 284.8 eV. Depth profiling experiments were also conducted to assess the concentration of each element through the thickness of the passive film by exposing the surface of each sample to a high energy flux of argon ions. The sputtering rate was estimated as 3 nm min^{-1}.

The corrosion behavior was studied by electrochemical impedance spectroscopy (EIS) and potentiodynamic polarization. Firstly, the working electrodes were prepared by connecting a copper wire to the rear surface of the specimen using a conductive colloidal silver paste to promote electrical contact. Next, the specimens were embedded in cold curing epoxy resin. After complete curing, surface preparation was performed by

mechanical grinding with waterproof silicon carbide papers, followed by polishing with diamond paste up to grit 1 μm. The electrochemical tests were conducted in a phosphate buffer saline (PBS) solution (pH = 7.2) at 37 °C using a potentiostat/galvanostat Autolab M101 A conventional three-electrode cell setup was employed with a platinum wire as the auxiliary electrode and Ag/AgCl as reference. Initially, the specimens remained immersed for 24 h to ensure a steady-state condition. After that, EIS measurements were made at the open circuit potential (OCP), in the frequency range from 100 kHz to 10 mHz, amplitude of the sinusoidal perturbation of ± 10 mV (rms) and an acquisition rate of 10 points per decade. Afterward, potentiodynamic polarization curves were obtained by sweeping the potential from − 300 mV with respect to the OCP up to + 1.0 $V_{Ag/AgCl}$ at a scanning rate of 1 mV s^{-1}. After polarization, the surfaces were observed by confocal laser scanning microscopy (Olympus, LEXT OLS4100).

The Mott-Schottky approach was employed to determine the semiconducting character and point defects density of the passive films formed on the ISO 5832-1 samples in the as-received and strained conditions. The experiments were conducted based on the same experimental setup described in the previous paragraph for the EIS and potentiodynamic polarization tests. Mott-Schottky plots were obtained at a fixed frequency of 1 kHz. The specimens were polarized in the cathodic direction at 50 mV successive steps from 500 $mV_{Ag/AgCl}$ up to − 1000 $mV_{Ag/AgCl}$. The dopants concentration was determined from the linear slopes of the $1/C^2$ versus E plots using the well-known Mott-Schottky equations (Eq 1 and 2). In these equations, C is the electrode capacitance, E is the applied potential, ε_0 is the vacuum permittivity ($\varepsilon_0 = 8.85 \times 10^{-14}$ F/cm), ε is the dielectric constant of the oxide film (12 for both the iron and chromium oxides), q is the electron charge (1.6×10^{-19} C), E_{FB} is the flat band potential, k is the Boltzmann constant and T is the absolute temperature (Ref 30). N_A and N_D are the acceptors and donors densities for a p-type and n-type semiconducting behavior, respectively.

$$\frac{1}{C^2} = -\frac{2}{\varepsilon \cdot \varepsilon_0 \cdot e \cdot N_A}\left(E - E_{FB} - \frac{kT}{e}\right) \quad \text{(Eq 1)}$$

$$\frac{1}{C^2} = \frac{2}{\varepsilon \cdot \varepsilon_0 \cdot e \cdot N_D}\left(E - E_{FB} - \frac{kT}{e}\right) \quad \text{(Eq 2)}$$

3. Results

3.1 Microstructural Characterization and Residual Stresses

CLSM micrographs of the as-received and strained samples are shown in Fig. 1. The micrographs were acquired in the longitudinal direction with respect to the applied stresses (same direction where the residual stresses were measured). The as-received microstructure (Fig. 1a) consists of small-sized austenitic grains, typical of biomedical austenitic stainless steels. After deformation, no significant microstructural alterations were observed for the strained samples (Fig. 1b-e).

The specimens subjected to tensile and compressive uniaxial deformations were tested with respect to the residual stresses developed at their surfaces. Residual stresses were measured by XRD along with the longitudinal axis with respect to the applied stresses. The results are shown in Fig. 2.

It is seen that the residual stresses generated by the uniaxial tensile tests are tensile in nature and increased with the deformation level. As expected, compressive residual stresses were generated at the samples exposed to the compressive tests. The nature of residual stresses is often linked to the corrosion response of metallic materials. In this respect, the role of surface stresses on the electrochemical behavior of strained stainless steel is central. The anodic reactivity upon immersion in chloride aqueous solutions is reported to be affected by mechanical straining (Ref 5). Compositional aspects of the passive film and its interaction with the generation and diffusion of point defects (oxygen vacancies, cation vacancies) must be taken into account to explain the effect of residual stresses on the corrosion behavior. Next sections deal with this subject.

3.2 XPS Analysis

3.2.1 Surface Chemical States. Figure 3 shows the XPS high-resolution spectra in the $Cr2p_{3/2}$, $Fe2p_{3/2}$, $Ni2p_{3/2}$, Mo3d and O1s regions for the passive film naturally formed on the surface of the as-received sample. The $Cr2p_{3/2}$ spectrum was fitted considering metallic chromium (Cr^0) and Cr^{3+} compounds (Cr_2O_3 and $Cr(OH)_3$). The binding energies are in accordance with other published reports on the passive film composition of stainless steels (Ref 31, 32). Chromium oxide displays a typical multiplet splitting (Ref 33). Deconvolution of the iron spectrum in the $Fe2p_{3/2}$ region showed the presence of five different states: metallic iron, Fe_3O_4, FeO, Fe_2O_3, FeOOH and also a high-energy surface peak of the Fe^{3+} valence state. Grosvenor et al. (Ref 34) give a detailed explanation for the origin of this peak. According to them, it is likely to be due to difference between the crystal field energy of Fe^{3+} ions in the surface and in the bulk material. Peak fitting of the nickel spectrum revealed the presence of metallic nickel and NiO and a small satellite peak at higher binding energies, as reported by other authors (Ref 35). The metallic component is the most intense one. It is frequently reported that, as a consequence of the lower oxidation tendency of nickel when compared to iron and chromium, the signal of the metallic state is high in the nickel spectrum of passive films formed on austenitic stainless steels (Ref 36). The presence of the metallic component is often associated with the photoelectrons emanating from the substrate (Ref 37). The Mo3d spectrum shows three doublets due to the presence of metallic molybdenum, Mo^{4+} and Mo^{6+} species in good agreement with the literature (Ref 38). In the O1s region, the spectrum was fitted considering two components associated with oxides (O^{2-}) and hydroxides (OH^-), as commonly found in the passive films of stainless steels (Ref 39). O^{2-} bonds predominate over OH^-, indicating the passive film of the as-received sample is mainly composed of oxide species.

Some differences are noticeable in the high-resolution spectra of the deformed samples with respect to the as-received material. The XPS $Cr2p_{3/2}$, $Fe2p_{3/2}$, $Ni2p_{3/2}$, Mo3d and O1s core levels are shown in Fig. 4 for the 15%T sample. The spectra for the other deformed samples (not shown) present the same compounds. At a first glance, therefore, the different deformation levels or modes did not affect the surface chemical states of the passive film in a significant way, since the same compounds were found either for the samples subject to tensile or compressive deformation at 15 and 30% levels.

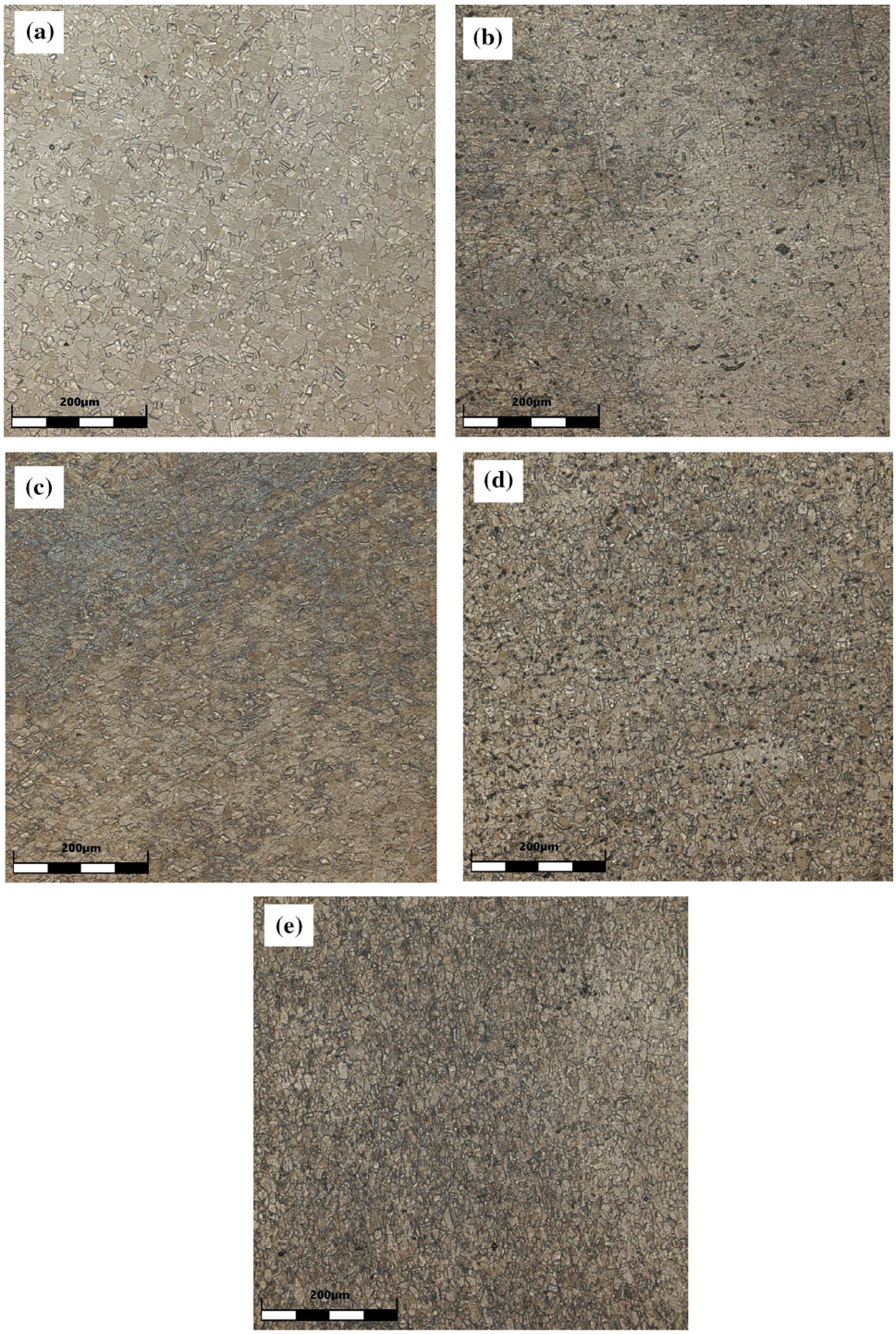

Fig. 1 CLSM micrographs of the NBR ISO 5832-1 stainless steel samples: (a) As-received; (b) 15%T; (c) 30%T; (d) 15%C; (e) 30%C

The same compounds found in the as-received sample (Fig. 3a) were present in the $Cr2p_{3/2}$ region of the 15%T sample (Fig. 4a), metallic chromium (Cr^0), Cr_2O_3 and $Cr(OH)_3$. The relative concentration of the metallic component is higher than for the as-received alloy, thus suggesting the passive film is thinner. The same finding was observed for the other deformed samples. A similar situation applies for the $Fe2p_{3/2}$ region. The oxidized iron compounds of the 15%T sample are the same of those found in the spectrum of the as-received steel (Fe_2O_3, Fe_3O_4, FeO and FeOOH), showing a mixture of Fe^{2+} and Fe^{3+} species. Metallic iron appears at a higher relative fraction in the spectra of the deformed alloys. The high-energy surface peak of Fe^{3+} was not found in the spectra of the deformed samples, suggesting that the difference of the crystal field energy of the Fe^{3+} ions in the surface and in the bulk material was not sustained when the alloy was mechanically deformed. The $Ni2p_{3/2}$ spectrum of the deformed samples (Fig. 4c) presents $Ni(OH)_2$ as an additional compound when compared to the as-

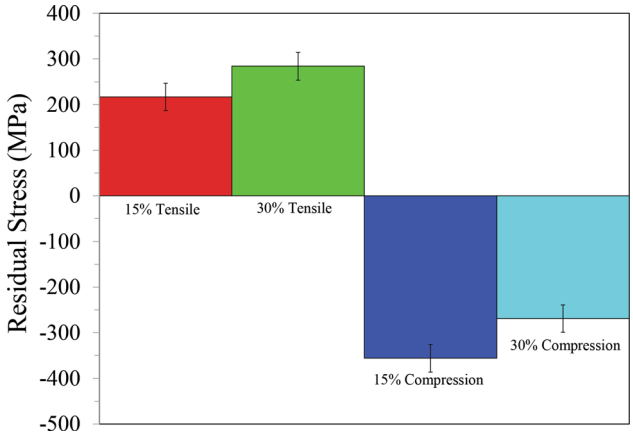

Fig. 2 Residual stresses of the NBR ISO 5832-1 samples at different loading modes and deformation levels

received samples. Its absence on the surface of the as-received alloy suggests it is less hydrated with respect to the deformed samples.

In order to confirm this hypothesis, the O1s spectra of the deformed samples were also deconvoluted, as shown in Fig. 4e for the 15%T sample. O^{2-} and OH^{-} bonds are the major components, as also found in the as-received surface. However, adsorbed water (H_2O_{ads}) is also present as a higher binding energy component at relative concentration of approximately 13%, thus revealing the most hydrated nature of the passive film formed on the mechanically strained samples.

The Mo3d spectrum of the T15% sample (Fig. 4d) exhibits the presence of metallic molybdenum (Mo^0) and a mixture of two oxidized species, Mo^{2+} and Mo^{4+} whereas Mo^{6+} was not found. That is the main difference between the spectra of the deformed and as-received samples in the Mo3d region. Mo^{2+} species are reported to be a minor part of the passive films on Mo-containing stainless steels (Ref 40), along with Mo^{4+} and Mo^{6+} compounds. The absence of Mo^{6+} on the deformed samples suggests the passive film formed after mechanical straining is in a less oxidized state which is probably associated with the more intense hydrated nature when compared to the as-received steel.

3.2.2 Depth Profiles. XPS depth profile of the passive films formed on the different NBR ISO 5832-1 samples is shown in Fig. 5. The as-received sample (Fig. 5a) presents higher oxygen concentration than for the metallic elements at the initial time. For all deformed samples, by contrast, iron concentration suppresses that of oxygen at the initial time, revealing the more oxidized nature of the passive film of the pristine surface when compared to the mechanically stressed samples.

As the passive film is removed, oxygen concentration greatly drops off and reaches near zero after 1200 s for the as-received sample. This sharp decrease of the oxygen concentration occurs faster for the deformed samples, suggesting its passive film is thinner. The higher signal of the metallic species observed in their high-resolution spectra (Fig. 4) is probably associated with this feature.

Iron is the most abundant metallic element in the passive film of all samples, since it is the major element of the steel composition and it is easily oxidized (Ref 41). As the passive film is removed, its content gradually increases, reaching an approximately stable plateau after the initial sputtering cycles, remaining mainly unchanged up to the end of the experiment. Such stable plateau of the iron concentration is reached after longer sputtering times for the pristine surface, likely due to its thicker passive layer, as also pointed by the variation of the oxygen concentration.

The chromium concentration is lower at the surface for all samples and increases with the sputtering time, indicating it is enriched in the inner part of the passive film. This effect mirrored that reported by other authors (Ref 42). It is also remarkable that its concentration is higher on the surface of the deformed samples when compared to the as-received one, suggesting the passive film stability could be enhanced by the previous mechanical straining step.

It is frequently reported that nickel is not associated with the passive film stability of stainless steels, being a small fraction of the oxide layer (Ref 43, 44). The relative high nickel concentrations observed in the depth profiles of all samples are likely due to two effects: the relative strong signal of the metallic component, as observed in the high-resolution spectra shown in Fig. 3(d) and 4(d) and also the thin nature of the passive films, giving rise to a relevant contribution of the substrate to the detected photoelectrons.

Molybdenum is practically absent in the initial time for the pristine surface (as-received sample, Fig. 5a), being detected in the inner parts of the passive film. By contrast, although it is the minor component, it is present at higher concentrations in the outer part of the passive films formed on the mechanically stressed samples. It is not possible to notice significant differences between the molybdenum contents of the outer and inner parts, in spite of a slight enrichment after the first sputtering cycle. Molybdenum, in spite of its relatively low concentration in the passive film of austenitic stainless steels, exerts a strong influence in the pitting corrosion ability. It is well-known that Mo species in the outer part of the passive film enhance the formation of the passivating Cr_2O_3 compound, thus enabling the formation of more stable passive film against the growth of stable corrosion pits (Ref 45). The molybdenum enrichment in the outer part of the passive films of the deformed samples is, therefore, a primary indication of its possible beneficial effect to improving their corrosion resistance.

Additional evidences on the different compositions of the passive films of the as-received and deformed samples can be observed based on the Cr/Fe, Mo/Fe and Ni/Fe ratios calculated from the depth profiles shown in Fig. 5. The results are displayed in Fig. 6.

The Cr/Fe ratio (Fig. 6a) is higher for the deformed samples, especially in the inner part of the passive films, as indicated by its remarkable increase after the first sputtering cycle whereas its ascending trend is not as marked for the as-received surface. The Mo/Fe ratio, in turn, presents an opposite trend (Fig. 6b). In spite of its ascending trend with the sputtering time, which resembles that of the Cr/Fe ratio, the increase rate is less marked for the deformed samples. Furthermore, the surface of the deformed samples is much more enriched in Mo than the pristine surface. Notwithstanding, this situation does not hold for the inner part of the passive films. As seen in Fig. 6(b), the Mo concentration is rather similar either for the as-received or deformed samples after the first sputtering cycle. The Ni/Fe ratio follows a similar trend. It is higher for the deformed samples at the initial time but, after the first sputtering cycles it is not possible to observe significant differences between its value for the as-received and deformed samples.

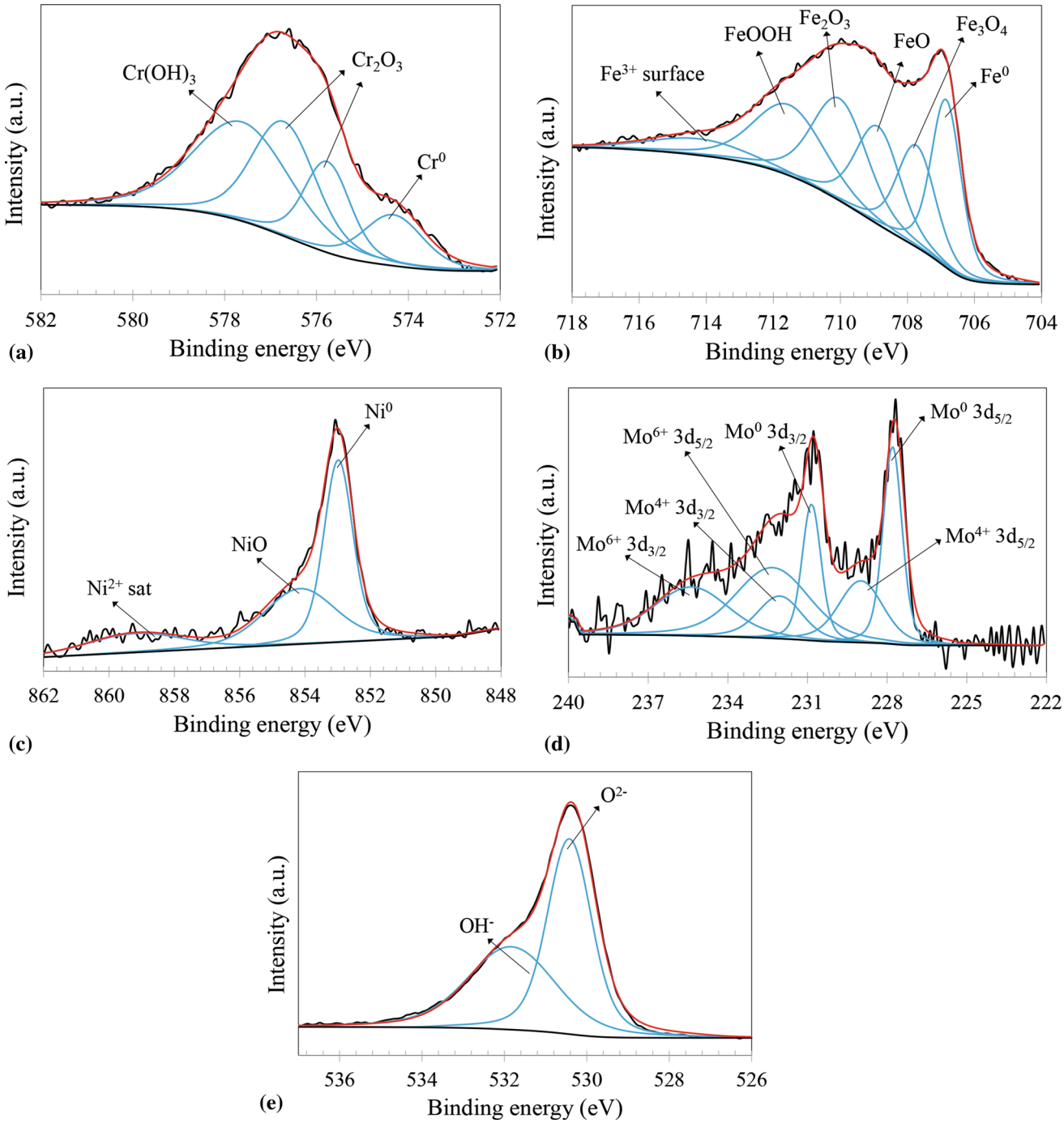

Fig. 3 XPS core levels of the passive film formed on the surface of the as-received sample: (a) $Cr2p_{3/2}$; (b) $Fe2p_{3/2}$; (c) $Ni2p_{3/2}$; (d) Mo3d; (e) O1s

3.3 Electrochemical Tests

3.3.1 Corrosion Behavior. Before EIS measurements, the open circuit potential (OCP) of the as-received and strained NBR ISO 5832-1 samples was monitored with the immersion time in PBS solution at 37 °C. The results are shown in Fig. 7. There is a general ascending trend of the OCP in the beginning of the monitoring period for all samples which is typically associated with the thickening of passive films in aqueous electrolytes (Ref 46). After 600 s, the potential tends to stabilize. It is noticeable that the OCP of the strained samples was shifted to more anodic values, suggesting an ennoblement of the passive film after deformation, either of tensile or compressive nature.

The EIS response of the as-received and strained NBR ISO 5832-1 samples was assessed after 24 h of immersion in PBS solution at 37 °C. Nyquist plots are shown in Fig. 8. The plots present one single capacitive loop that is little depressed in the low-frequency domain. This behavior is typical of surgical stainless steels in simulated biological fluids (Ref 47, 48), being associated with the high stability of the passive film (Ref 49). The diameter of the capacitive loop is related to the charge

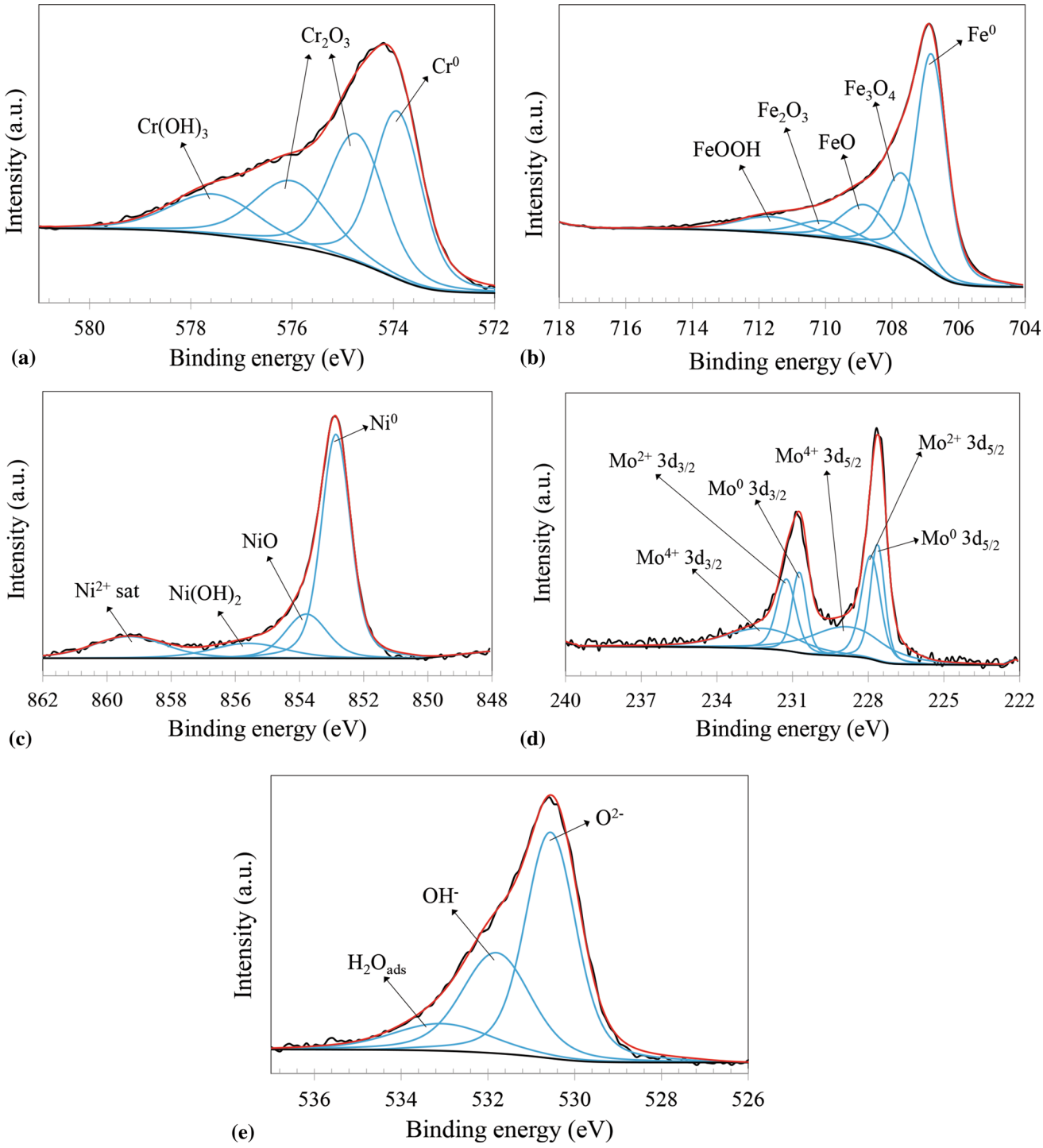

Fig. 4 XPS core levels of the passive film formed on the surface of the 15%T sample: (a) Cr2$p_{3/2}$; (b) Fe2$p_{3/2}$; (c) Ni2$p_{3/2}$; (d) Mo3d; (e) O1s

transfer resistance of the electrode/electrolyte interface and can be used to qualitatively express its corrosion resistance (Ref 50, 51). In this respect, the results point to a slight increase of the corrosion resistance of the NBR ISO 5832-1 stainless steel after deformation. In the strained state, either tensile or compressive, the capacitive loop diameter increased when compared to the as-received sample.

Potentiodynamic polarization curves of the as-received and strained NBR ISO 5832-1 samples after 24 h of immersion time in PBS solution at 37 °C are displayed in Fig. 9. The values of corrosion potential E_{corr} were determined from these curves. All samples present a typical passive response as denoted by the wide potential range where the current density remains approximately constant with the applied potential, above E_{corr}. In this case, the anodic dissolution rate can be related to the passive current density (i_{pass}). In the present work, the values of i_{pass} were considered at the middle of the passive range, as also adopted by other authors (Ref 52). It was not possible to observe a breakdown potential in the polarization curves shown in Fig. 9. The steep increase of the current density right above

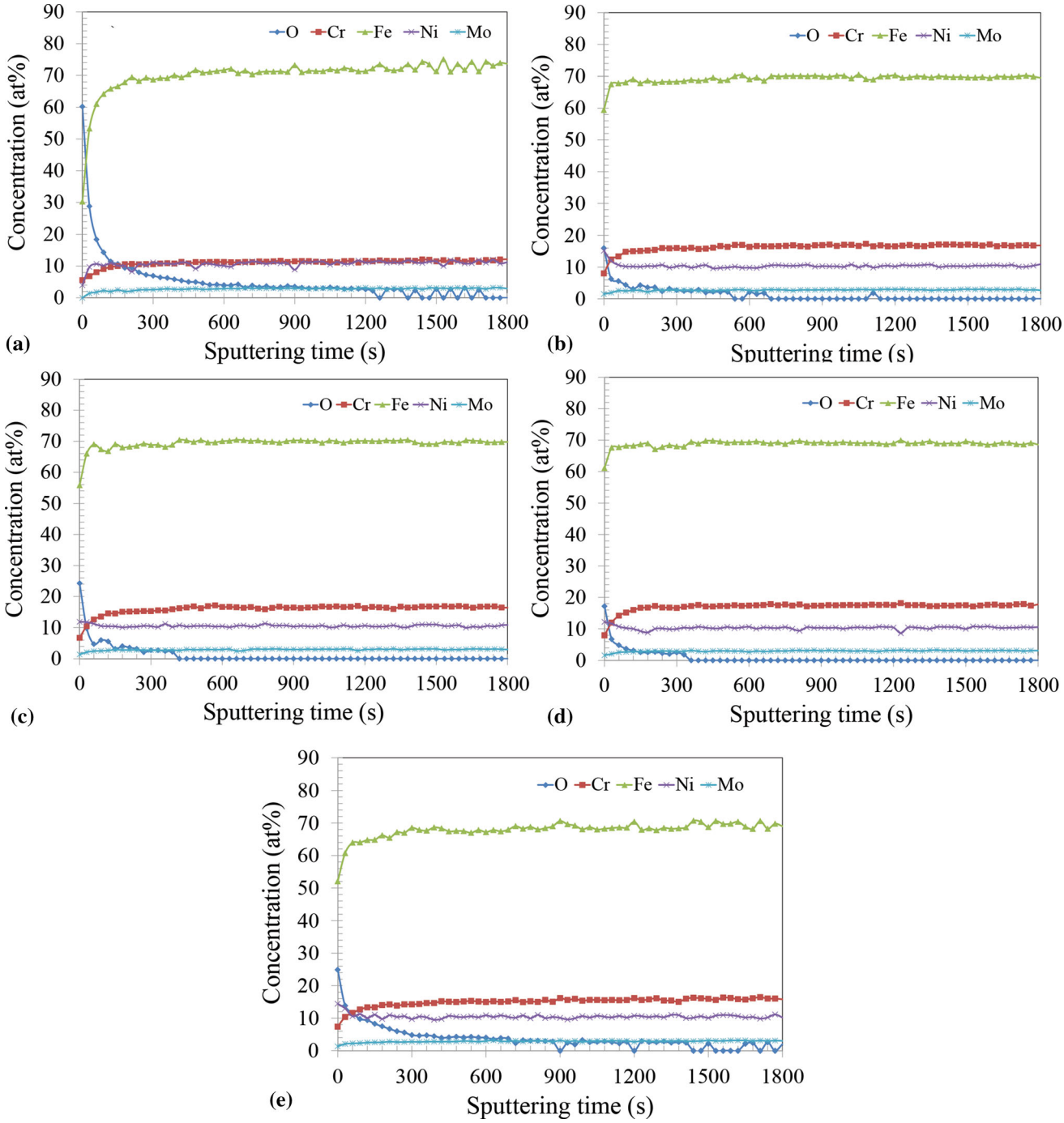

Fig. 5 XPS depth profiles of the NBR ISO 5832-1 stainless steel samples: (a) As-received; (b) 15%T; (c) 30%T; (d) 15%C; (e) 30%C

1.0 $V_{Ag/AgCl}$ is rather related to the oxygen evolution reaction than to the onset of stable pit propagation. The passive range was, therefore, considered as the difference between the potential at which the steep increase of the current density started and E_{corr}. These values are shown in Table 1, along with i_{pass} and E_{corr} values.

The corrosion potential was little affected by deformation, as denoted by the small variation of E_{corr} of the strained samples when compared to the as-received condition. All polarization curves are typically passive, independently of the deformation mode. The anodic current densities remained relative stable throughout a wide passive range. The transpassive region occurs at similar potentials for all samples, just above +1.0 $V_{Ag/AgCl}$, which is likely to be due to the oxygen evolution reaction. The passive ranges are wide and were not significantly affected by deformation. The most striking feature is the decrease of the anodic dissolution rate of the strained samples with respect to the as-received alloy. As seen in Table 1, the value of i_{pass} decreased after deformation, especially for the 15%C sample. This result is in accordance with the Nyquist plots shown in Fig. 8, indicating slower corrosion kinetics for the 15%C condition.

Figure 10 shows CLSM micrographs of the as-received and strained samples, after the potentiodynamic polarization tests.

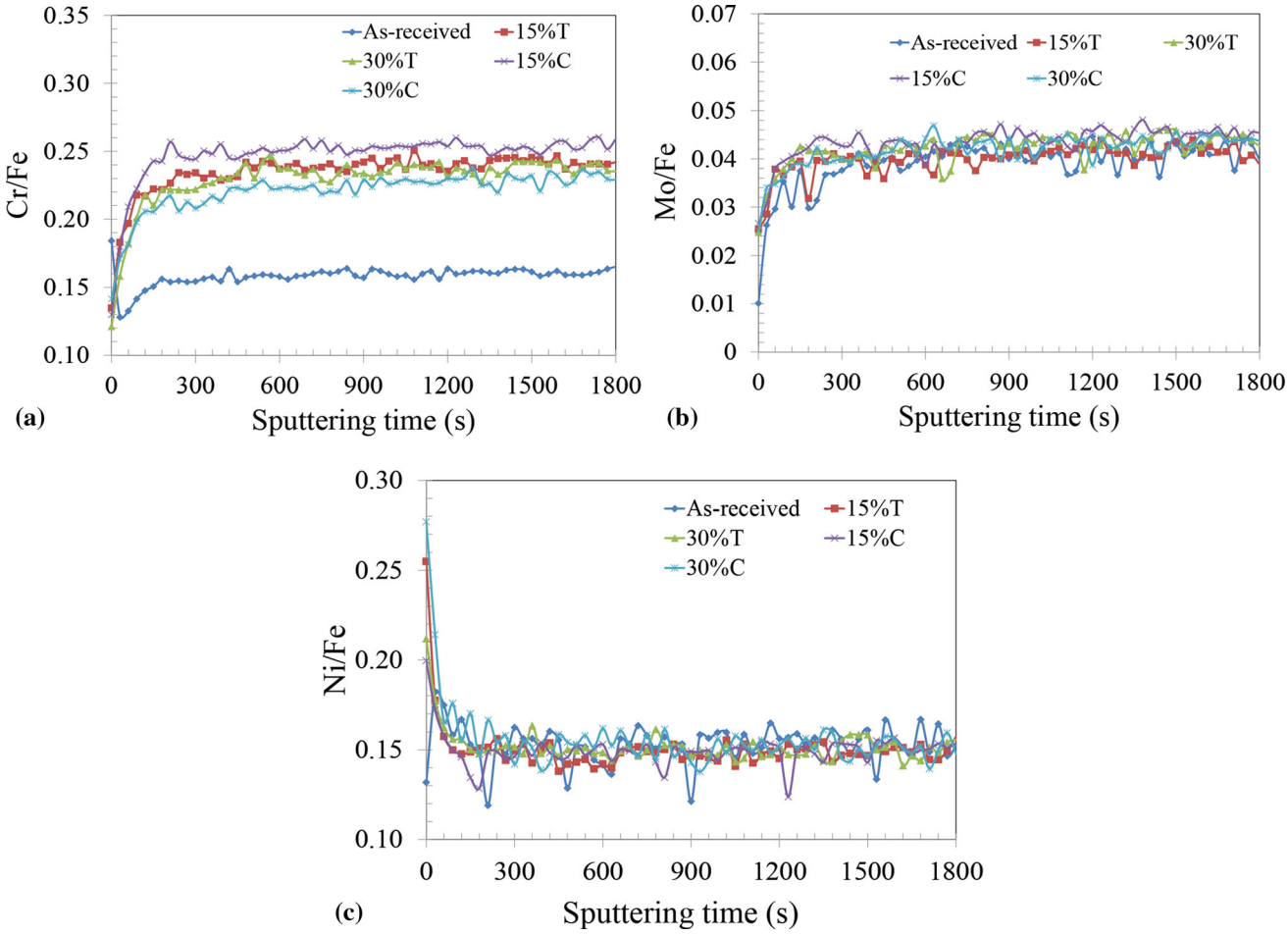

Fig. 6 (a) Cr/Fe; (b) Mo/Fe and (c) Ni/Fe ratios obtained from the depth profile shown in Fig. 4

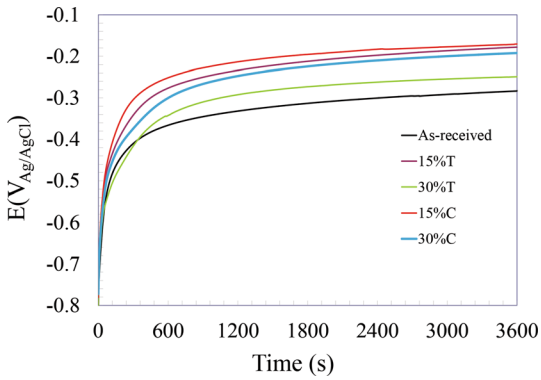

Fig. 7 Variation of the OCP of the as-received and strained NBR ISO 5832-1 samples with the immersion time in PBS solution at 37 °C

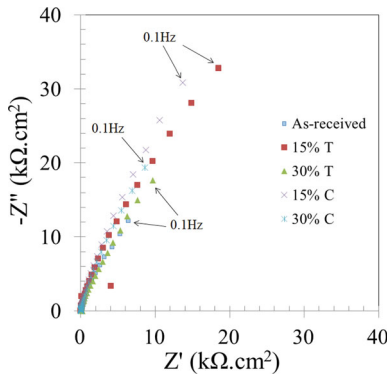

Fig. 8 Nyquist plots of the as-received and strained NBR ISO 5832-1 samples after 24 h of immersion time in PBS solution at 37 °C

The corrosion morphology is typically characterized by the presence of small pits on the polarized samples. The number of pits is especially high in the as-received steel, as shown in Fig. 10(a). The samples subject to compressive residual stresses displays fewer pits when compared to the 15%T (Fig. 10c) and 30%T (Fig. 10e) samples, especially the 15%C sample (Fig. 10b), giving additional evidence of its superior corrosion resistance.

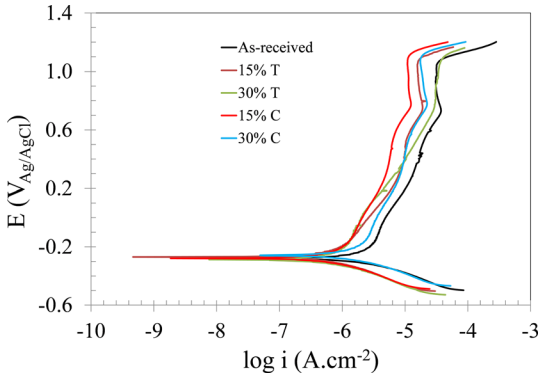

Fig. 9 Potentiodynamic polarization curves of the as-received and strained NBR ISO 5832-1 samples after 24 h of immersion time in PBS solution at 37 °C

Table 1. Corrosion parameters determined from the potentiodynamic polarization curves shown in Fig. 9

Sample	i_{pass}, µA/cm^2	Passive range, $mV_{Ag/AgCl}$	E_{corr}, $mV_{Ag/AgCl}$
As-received	15.1	1362	− 278
15% T	8.5	1330	− 269
30% T	8.1	1401	− 287
15% C	5.6	1387	− 279
30% C	9.5	1384	− 260

3.3.2 Semiconducting Character of the Passive Films. The semiconducting character of the passive films is important to the corrosion resistance of metallic materials, since it is related to the electronic properties and transport of ions through the oxide layer. Mott-Schottky plots of the as-received and strained NBR ISO 5832-1 samples after 24 h of immersion time in PBS solution at 37 °C are shown in Fig. 11. Acceptors (N_A) and donors (N_D) concentrations were determined from the linear portions of these plots. The results are displayed in Table 2. N_D values are obtained from the positive slopes whereas N_A are determined from the negative slopes.

From Fig. 11, the duplex character of the passive films formed on the as-received and strained samples is evident. The negative slopes are typical of p-type semiconducting behavior, being associated with compounds such as Cr_2O_3, FeO, MoO_2 and NiO for which the main charge carriers are cation vacancies (Ref 53, 54). At the more negative potentials, the Mott-Schottky plots change to a positive slope, indicating the transition to n-type semiconducting character (Ref 55). Oxygen vacancies and cation interstitials are the point defects that endow the passive film with n-type behavior typical of FeOOH and MoO_3 (Ref 53, 54). These species were identified by XPS, as shown in section 3.2.1.

According to Eq 1 and 2, the doping densities are inversely proportional to the slopes of the linear portions of the Mott-Schottky plots. There was, therefore, an obvious increase of the slopes of the linear portions for the deformed samples which are sharper for the samples subject to compressive stresses. As a consequence, as shown in Table 2, the charge carrier concentrations are higher in the passive film of the as-received sample when compared to the deformed ones. Moreover, the passive films formed under uniaxial compression present fewer defects than those formed under uniaxial tension.

4. Discussion

Cold work of the ISO 5832-1 surgical stainless steel subject to uniaxial tensile or compressive stresses promoted different electrochemical responses, depending on the nature of the uniaxial stress. As depicted in section 3.1, mechanical straining generated stresses whose signal and intensity were measured by x-ray diffraction. Correlation between corrosion of metallic materials and surface residual stresses has been investigated by several authors. For instance, Liu et al. (Ref 56) have found that compressive stresses increased the resistance to passive film rupture in an aluminum-copper alloy, thus reducing its susceptibility to localized corrosion. Peyre et al. (Ref 57) have reached a similar conclusion regarding the effect of compressive stresses on the corrosion resistance of 316L stainless steel. The results obtained in the present work point to the same direction.

In fact, the amount of deformation imparted by cold work is recognized to affect the corrosion resistance of austenitic stainless steels. Mudali et al. (Ref 58) observed an increase of the pitting corrosion resistance of 316L stainless steels up to 20% thickness reduction by cold rolling. As suggested by the authors such beneficial effect of plastic deformation would arise from an enhanced stability of the passive film derived from surface diffusion that compensates eventual deleterious effects of increased crystalline defects such as mechanical twins. The composition of the passive film was not determined, though.

Another important aspect of the benefits of compressive stresses to decreasing pitting corrosion susceptibility of stainless steels was investigated by Vignal et al. (Ref 59). They associated an increase of the corrosion resistance when surface residual stresses on 316L stainless steel samples subject mechanical loading were of a compressive nature. In contrast, tensile stresses present an opposite effect. According to the results, tensile stresses led to the formation of additional point defects in the passive film, increasing its conductivity and, therefore, its susceptibility to pitting corrosion. Hence, it can be argued that there is an undeniable correlation between the nature of the surface stresses and the semiconducting properties of the passive films on stainless steels. It is also possible to hypothesize that, upon considering the validity of such correlation, passive film composition must play a critical role in this scenario. Vignal et al. (Ref 59) recognize the importance of this issue to understand the interaction between the stress state and the corrosion resistance of stainless steels, since the conductivity of the oxide layer depends on its chemical composition. Nonetheless, detailed assessment of passive film composition is not provided.

In the light of the scenario depicted above, it is obvious that passive film composition must be fully known to enable a deep understanding on the complex interplay between deformation, residual stresses, electronic properties of the passive film and corrosion resistance of austenitic stainless steels. By taking into account the results shown in Fig. 6, the most relevant compositional differences between the samples were observed for the Cr/Fe ratios of the passive films whereas Mo/Fe and Ni/Fe ratios were similar for all samples. Therefore, it is

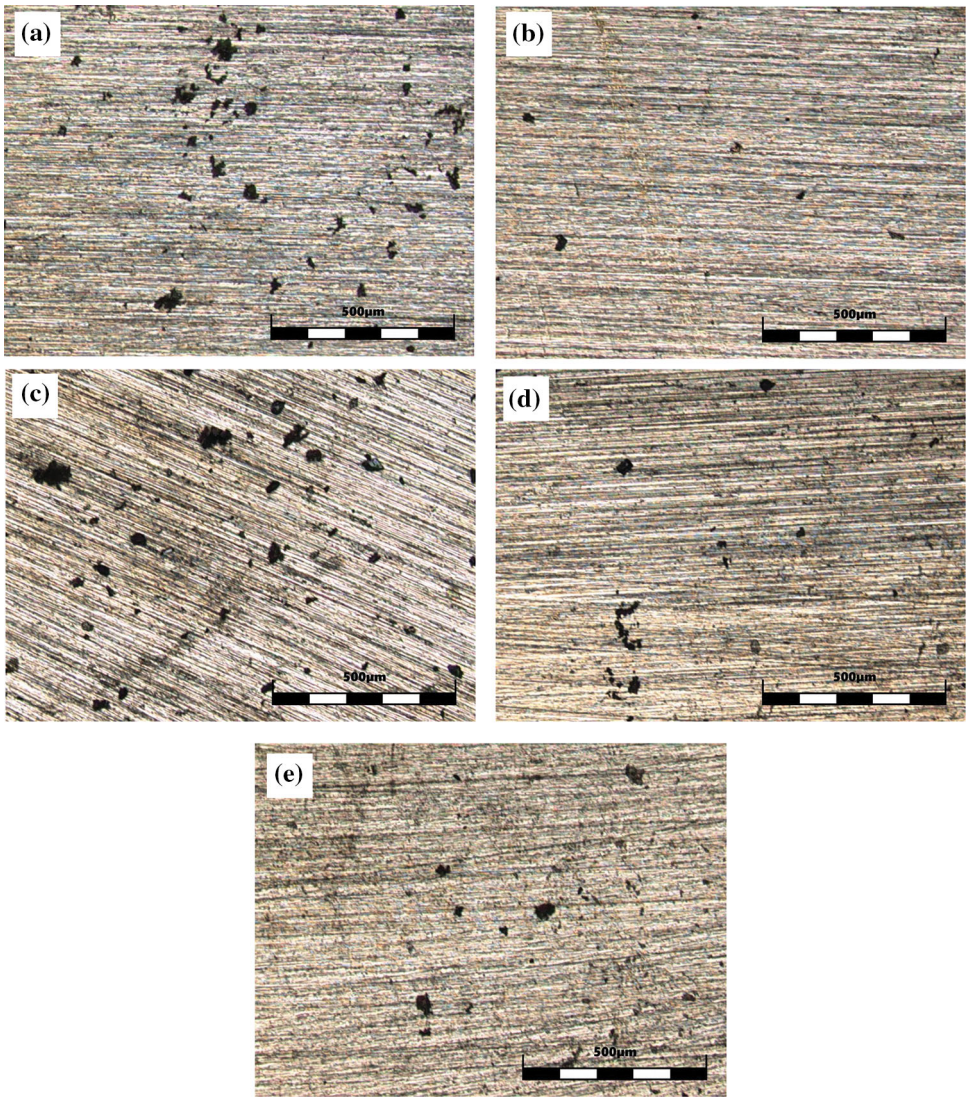

Fig. 10 CLSM micrographs of the NBR ISO 5832-1 samples after potentiodynamic polarization tests: (a) As-received; (b) 15%C; (c) 15%T; (d) 30%C; (e) 30%T

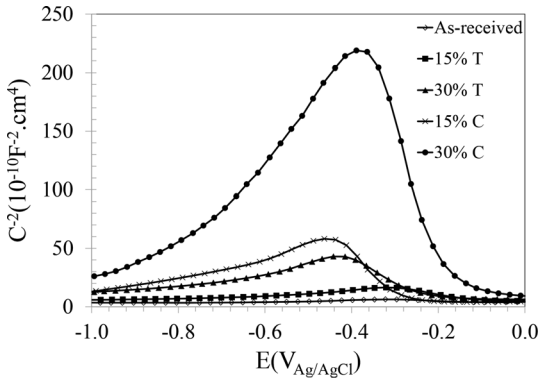

Fig. 11 Mott-Schottky plots of the as-received and strained NBR ISO 5832-1 samples after 24 h of immersion time in PBS solution at 37 °C

Table 2. Concentrations of charge carriers in the passive films of the as-received and strained NBR ISO 5832-1 samples after 24 h of immersion time in PBS solution at 37 °C

Sample	N_A, 10^{20} cm^{-3}	N_D, 10^{20} cm^{-3}
As-received	0.82	1.14
15% T	0.21	0.41
30% T	0.07	0.18
15% C	0.04	0.14
30% C	0.01	0.04

reasonable to assume that chromium species should present the most important influence on the electrochemical properties of the NBR ISO 5832-1 stainless steel samples. With the aim of elucidating these aspects in the context of the present work, we have deconvoluted the XPS spectra in the Cr $2p_{3/2}$ region for selected sputtering times during depth profiling experiments. According to the literature (Ref 41, 60), the passive film thickness is considered to be related to the 50% value of the maximum of oxygen amplitude in the XPS depth profiling results. From Fig. 5, oxygen concentration decreases more than

50% after 300 s sputtering for all samples. As a consequence, the spectra were deconvoluted up to a sputtering time of 300 s, as it should give the most relevant information about the passive film composition for all samples. The relative concentrations of chromium compounds were calculated from these spectra. The results are displayed in Fig. 12. As the main constituent of the alloy composition, iron is also an important part of the passive film of austenitic stainless steels. Hence, we have also deconvoluted the XPS spectra in the Fe $2p_{3/2}$ region at the same selected sputtering times. The relative fractions of iron compounds were calculated, and the results are displayed in Fig. 13.

Figure 12a gives unequivocal evidence that Cr^{3+} species are depressed in the inner regions of the passive film on the as-received sample. Metallic chromium, in turn, greatly increased with the sputtering time, indicating a rapid removal of the passivating $Cr(OH)_3$ and Cr_2O_3 oxidized species. Conversely, the strained samples presented a distinct distribution of chromium compounds through the thickness of the passive film. As seen in Fig. 12(b), the relative concentration of Cr_2O_3 at the surface (0 s) is much higher for the 15%C sample than for the as-received sample. Moreover, the inner layers of the passive film are enriched with Cr_2O_3, reaching a maximum at 150 s and the relative concentration of metallic chromium

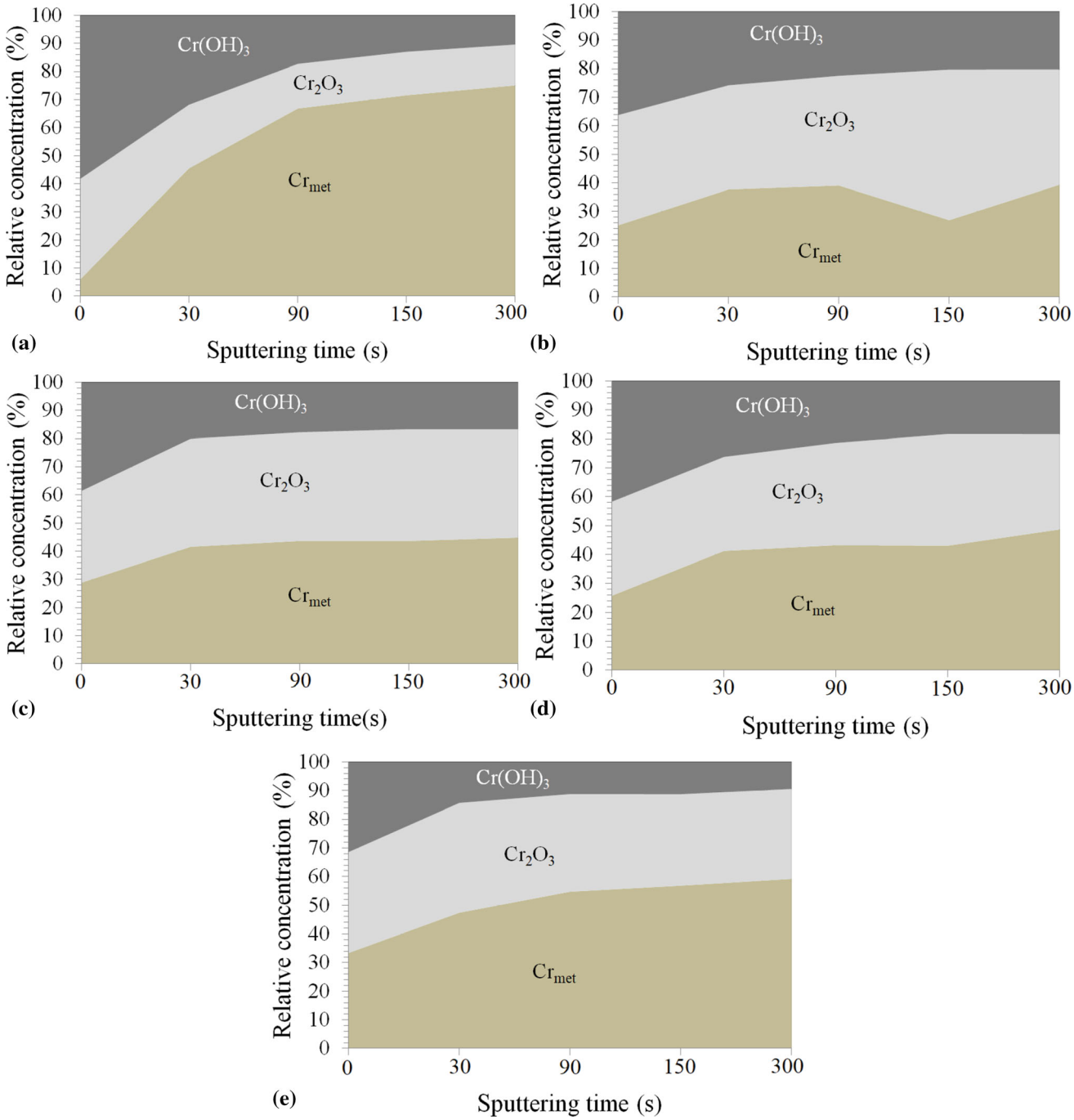

Fig. 12 Relative concentration of chromium species in the passive films of the NBR ISO 5832-1 samples as determined from deconvolution of XPS spectra at selected sputtering times: (a) As-received; (b) 15%C; (c) 15%T; (d) 30%C; (e) 30%T

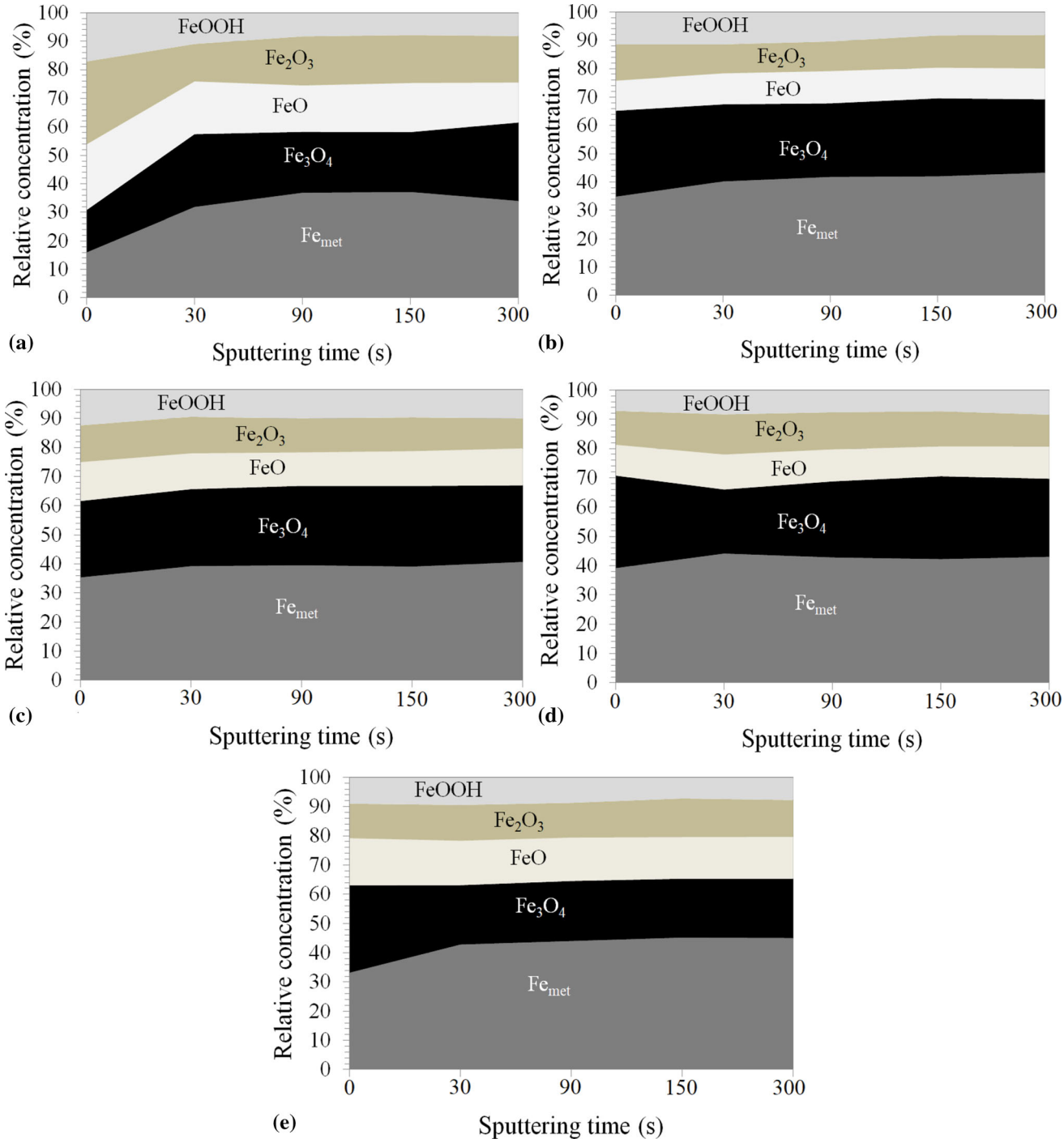

Fig. 13 Relative concentration of iron species in the passive films of the NBR ISO 5832-1 samples as determined from deconvolution of XPS spectra at selected sputtering times: (a) As-received; (b) 15%C; (c) 15%T; (d) 30%C; (e) 30%T

remained low up to 300 s with respect to the unstrained condition. Hence, it is suggested that the chromium hydroxide-rich passive layer of the as-received sample was more easily removed, leading to the observed rapid rise of the metallic chromium concentration as the substrate is more easily reached by the incident x-ray beam. He et al. (Ref 61) highlighted the effect of stress in the passive film composition of austenitic stainless steels with regard to the conversion of chromium hydroxide to chromium oxide and how the protective character of the oxide layer is affected by such transformation. Chromium hydroxide is the primarily formed at the surface and is partially converted to Cr_2O_3 by a de-hydration reaction. As the density of chromium hydroxide is lower than that of Cr_2O_3, a dense passive layer is expected to form at the interface between passive film and substrate, thus enhancing its corrosion protection ability. Moreover, this reaction leads to marked volumetric shrinkage of the oxide layer due to the different densities of hydroxide and oxide species that is favored when the material is subject to compressive stresses. Tensile stresses, in turn, would not favor such conversion. The improvement of

the corrosion resistance of the 15%C sample observed in the potentiodynamic polarization curves shown in Fig. 9 could derive from such effect, due to the Cr_2O_3 enrichment experienced by the passive film under the compressive stress field. Notwithstanding, by increasing the amount of compressive stress to 30%, the corrosion resistance was not further improved, as also shown in section 3.3.1. This could be due to the fact that the residual compressive stresses were not intensified when the compressive deformation was raised to 30% (Fig. 2), thus not rendering the passive film enriched with Cr_2O_3 when compared to the 15%C condition. In fact, the relative amount of Cr_2O_3 in the passive film of the 30%C sample (Fig. 12d) is apparently lower than that of the 15%C sample (Fig. 12b). Similarly, Cr_2O_3 enrichment of the passive films of the samples subject to tensile tests was not as marked as that of the 15%C. Figure 12(c) (15%T) and (e) (30%T) points to an enrichment of Cr_2O_3 with respect to the as-received sample, but it does not surpass the amount of chromium oxides in the oxide layer of the 15%C sample.

By examining the results exhibited in Fig. 13, one major difference between the as-received and the strained samples is related to the relative concentration of the iron oxidized species at the surface (0 s). As clearly indicated in Fig. 13(a), the fraction of oxidized species (Fe_3O_4, FeO, Fe_2O_3 and FeOOH at the surface of the as-received alloy surpasses that on the strained samples, either for those subject to tensile or compressive stresses. Moreover, while Fe_2O_3 and FeO predominate on the as-received sample, Fe_3O_4 is the main compound on all strained samples. Indeed, magnetite predominates not only on the very first surface but also over the whole sputtering range for the strained samples, as observed in Fig. 13(b) to (e), although the main difference with respect to the as-received condition resides on the non-sputtered surface (0 s). For longer sputtering times, magnetite is the major oxidized iron compound within the passive layer for all samples. The less corrosion protective FeOOH (Ref 62) did not present significant compositional differences for any sample.

In spite of being a major part of the passive film, iron compounds are not expected to critically influence its corrosion resistance, as chromium species are the main passivating agents (Ref 61). In fact, our results did not permit to observe a clear correlation between the stress state, the relative concentration of iron compounds in the passive film and the corrosion resistance of the NBR ISO 5832-1 stainless steel samples. Notwithstanding, one important aspect of the passive film stability is related to the ratio between Cr_2O_3 and the less protective iron oxides/hydroxides at the surface and through the thickness of the oxide layer. By calculating such ratio (Cr_2O_3/Fe_{oxid}) for the same selected sputtering times, additional differences between the composition of the passive films formed on the as-received and strained samples can be more clearly evaluated. These results are, therefore, displayed in Fig. 14.

From Fig. 14, it is clear that iron compounds are the major constituents of the passive films on all samples. Furthermore, there is a strong Cr_2O_3 enrichment in the inner parts of the passive films of all strained samples with respect to the as-received alloy. Such enrichment is remarkable for the 15%C sample, as seen at the sputtering time of 150 s for which the Cr_2O_3/Fe_{oxid} ratio reached its maximum value. In one hand, the compressive stress can be considered to enhance chromium diffusion through the passive film, thus enabling the Cr_2O_3 enrichment. As a consequence, the corrosion resistance was improved, as seen in section 3.3.1. However, further increasing

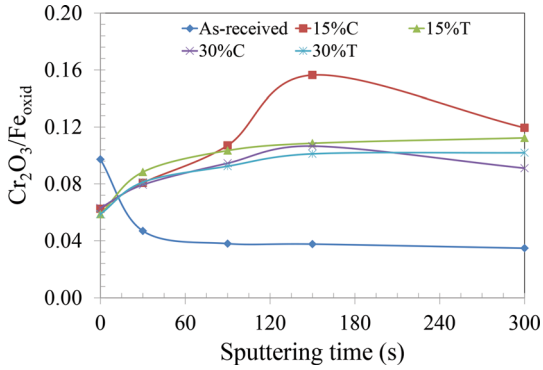

Fig. 14 Ratio between Cr_2O_3 and oxidized iron species in the passive films of the NBR ISO 5832-1 samples obtained from XPS depth profiles at selected sputtering times

the amount of deformation under compression to 30% (30%C) did not led to a corresponding increase of the Cr_2O_3/Fe_{oxid} ratio. Tensile stresses (15%T and 30%T) have also shown Cr_2O_3 enrichment with respect to the as-received sample, but it was not as marked as that of the 15%C sample.

The semiconducting properties of the passive film are also affected by its composition, giving rise to strict interdependence with the corrosion resistance. It is, therefore, important to assess the correlation between the stress state, passive film composition and the concentration of point defects determined from the Mott-Schottky plots (section 3.3.2). The point defect model (PDM) assumes that oxygen vacancies and cations interstitials act as n-type dopants whereas p-type behavior is related to predominance of cation vacancies as the main dopants (Ref 63). The dominant donors in the passive films are considered to be oxygen vacancies (Ref 55). As highlighted by Zhang et al. (Ref 64), upon increasing the concentration of oxygen vacancies the passive film becomes more defective, thus disrupting its stability. Cr^{3+} ions are reported to have preferential affinity by oxygen atoms, repairing the passive film and help maintaining high corrosion resistance (Ref 65). According to the literature, the donor density can be envisaged as a measure of the affinity of the passive film for chloride ions, being correlated with the pitting corrosion resistance (Ref 66). Increasing the concentration of point defects with n-type semiconductivity should decrease the stability of the passive film.

Although the influence of the stress level on the concentrations of donors (N_D) and acceptors (N_A) is not so obvious from Table 2, the increased N_D value of the as-received condition when compared to the strained samples is clear. Moreover, there is an increasing trend of the donor density for the specimens subject to tension tests when compared to the compressed samples at the same strain level. In the light of the PDM, these results could indicate two important aspects. Firstly, deformation unequivocally affected the electronic properties of the passive film which is much likely related to the passive film composition, as denoted by the Cr_2O_3 enrichment with respect to the oxidized iron species (Fig. 14) that are mainly of n-type character, such as Fe_3O_4, Fe_2O_3 and FeOOH (Ref 67). As a consequence, the corrosion resistance of the deformed samples depended on both the passive film composition and electronic properties of the passive film which are both influenced by the stress state. Secondly, this scenario seems to be affected by the nature of the surface residual

stresses, tensile or compressive. Tensile stresses did not favor the formation of the passivating Cr_2O_3 compound as much as the compressive ones, especially for those deformed at 15%. The increase of n-type defects concentration was also triggered by the tensile stresses with respect to the compressed samples. As a consequence, susceptibility to corrosion due to the more defective passive film is expected. Indeed, the results of the electrochemical tests confirm such expectation, revealing the improved corrosion resistance of the 15%C condition for which the passive film was the most enriched with Cr_2O_3 and with low concentration of n-type point defects. Whichever the factor that predominates, our results confirm that there is an interaction between uniaxial stress loading, passive film composition, corrosion resistance and electronic properties of the passive film is on the NBR ISO 5832-1 samples. Compression strain seems to be an interesting route to tailor the surface properties of the steel toward enhanced passive film stability.

5. Conclusions

Uniaxial stress loading affected the corrosion behavior of the NBR ISO 5832-1 stainless steel. A complex interaction between stress state, chemical composition and electronic properties of the passive film could be realized. The main conclusions are given as follows:

(a) The sample with the most intense compressive residual stresses (15%C) displayed the lowest passive current density and concentration of electron donors, indicating its slower corrosion kinetics and high passive film stability when compared to the as-received steel and samples with tensile residual stresses.
(b) XPS analysis showed that the compressed samples were more enriched with the passivating Cr_2O_3 compound when compared to the samples with surface tensile stresses. Compressive stresses triggered the formation of Cr_2O_3, improving the passive film stability.
(c) The stress state did not influence the composition of the passive film with respect to Fe, Mo and Ni species. As a consequence, the corrosion resistance was not significantly affected by these species. Its main effect was related to Cr_2O_3 enrichment that was triggered for the compressed samples.

Acknowledgments

Authors are thankful to CAPES for the financial support (Finance Code 001) and to the Experimental Multiuser Facilities (UFABC) for the experimental support to this work.

References

1. G. Monrrabal, A. Bautista, S. Guzman, C. Gutierrez and F. Velasco, Influence of the Cold Working Induced Martensite on the Electrochemical Behavior of AISI 304 Stainless Steel Surfaces, *J. Mater. Res. Technol.*, 2014, **8**, p 1335–1346
2. E. Jafari, Corrosion Behaviors of Two Types of Commercial Stainless Steel After Plastic Deformation, *J. Mater. Sci. Technol.*, 2010, **26**, p 833–838
3. O. Söderberg, X.W. Liu, P.G. Yakovenko, K. Ullakko and V.K. Lindroos, Corrosion Behavior of Fe-Mn-Si Based Shape Memory Steel Strained by Cold Rolling, *Mater. Sci. Eng. A*, 1999, **273–275**, p 543–548
4. Y. Hou, Y. Li, C. Zhang, Y. Koizumi and A. Chiba, Effects of Cold Working on Corrosion Resistance of Co-Modified Ni-16Cr-15Mo Alloy in Hydrofluoric Acid Solution, *Corros. Sci.*, 2014, **89**, p 257–267
5. Y. Boudinar, K. Belmokre, M. Touzet, O. Devos and M. Puiggali, Investigation of the Passivation Process of Plastically Deformed 316L Stainless Steel Using the High Frequency Capacitance Obtained by EIS, *Mater. Corros.*, 2019, **70**, p 206–215
6. B. Ravi Kumar, B. Mahato and R. Singh, Influence of Cold-Worked Structure on Electrochemical Properties of Austenitic Stainless Steels, *Metall. Mater. Trans. A Phys. Metall. Mater. Sci.*, 2007, **38**, p 2085–2094
7. H. Wu, C. Li, K. Fang, W. Zhang, F. Xue, G. Zhang and X. Wang, Effect of Residual Stress on the Stress Corrosion Cracking in Boiling Magnesium Chloride Solution of Austenite Stainless Steel, *Mater. Corros.*, 2018, **69**, p 1572–1583
8. S.G. Acharyya, A. Khandelwal, V. Kain, A. Kumar and I. Samajdar, Surface Working of 304L Stainless Steel: Impact on Microstructure, Electrochemical Behavior and SCC Resistance, *Mater. Charact.*, 2012, **72**, p 68–76
9. A. Nazarov, V. Vivier, F. Vucko and D. Thierry, Effect of Tensile Stress on the Passivity Breakdown and Repassivation of AISI 304 Stainless Steel: A Scanning Kelvin Probe and Scanning Electrochemical Microscopy Study, *J. Electrochem. Soc.*, 2019, **166**, p C3207–C3219
10. L.V. Jin-long and L. Hong-Yun, Influence of Tensile Pre-strain and Sensitization on Passive Films in AISI 304 Austenitic Stainless Steel, *Mater. Chem. Phys.*, 2012, **135**, p 973–978
11. Q. Yang and J.L. Luo, Effects of Hydrogen and Tensile Stress on the Breakdown of Passive Films on Type 304 Stainless Steel, *Electrochim. Acta*, 2001, **46**, p 851–859
12. Y. Fu, X. Wu, E.H. Han, W. Ke, K. Yang and Z. Jiang, Effects of Cold Work and Sensitization Treatment on the Corrosion Resistance of High Nitrogen Stainless Steel in Chloride Solutions, *Electrochim. Acta*, 2009, **54**, p 1618–1629
13. X. Feng, X. Lu, Y. Zuo and D. Chen, The Passive Behaviour of 304 Stainless Steels in Saturated Calcium Hydroxide Solution Under Different Deformation, *Corros. Sci.*, 2014, **82**, p 347–355
14. A.H. Ramírez, C.H. Ramírez and I. Costa, Influence of Cold Deformation on Pitting Corrosion Resistance of ISO NBR 5832-1 Austenitic Stainless Steel Used for Orthopedic Implants, *J. Braz. Chem. Soc.*, 2014, **25**, p 1270–1274
15. A.H. Ramírez, C.H. Ramírez and I. Costa, Cold Rolling Effect on the Microstructure and Pitting Resistance of the NBR ISO 5832-1 Austenitic Stainless Steel, *Int. J. Electrochem. Sci.*, 2013, **8**, p 12801–12815
16. J. Lv, T. Liang, C. Wang and T. Guo, Effect of in Site Strain on Passivated Property of the 316L Stainless Steels, *Mater. Sci. Eng. C*, 2016, **61**, p 32–36
17. M. Talha, C.K. Behera and O.P. Sinha, In-Vitro Long Term and Electrochemical Corrosion Resistance of Cold Deformed Nitrogen Containing Austenitic Stainless Steels in Simulated Body Fluid, *Mater. Sci. Eng. C*, 2014, **40**, p 455–466
18. S. Ramya, T. Anita, H. Shaikh and R.K. Dayal, Laser Raman Microscopic Studies of Passive Films Formed on Type 316LN Stainless Steels During Pitting in Chloride Solution, *Corros. Sci.*, 2010, **52**, p 114–121
19. S.V. Phadnis, A.K. Satpati, K.P. Muthe, J.C. Vyas and R.I. Sundaresan, Comparison of Rolled and Heat Treated SS304 in Chloride Solution Using Electrochemical and XPS Techniques, *Corros. Sci.*, 2003, **45**, p 2467–2483
20. A.S. Hamdy, E. El-Shenawy and T. El-Bitar, The Corrosion Behavior of Niobium Bearing Cold Deformed Austenitic Stainless Steels in 3.5% NaCl Solution, *Mater. Lett.*, 2007, **61**, p 2827–2832
21. S. Ghosh, V.P.S. Rana, V. Kain, V. Mittal and S.K. Baveja, Role of Residual Stresses Induced by Industrial Fabrication on Stress Corrosion Cracking Susceptibility of Austenitic Stainless Steels, *Mater. Des.*, 2011, **32**, p 3823–3831
22. A.B. Rhouma, C. Braham, M.E. Fitzpatrick, J. Lédion and H. Sidhom, Effects of Surface Preparation on Pitting Resistance, Residual Stress, and Stress Cracking in Austenitic Stainless Steels, *J. Mater. Eng. Perform.*, 2001, **10**, p 507–514

23. N. Ouali, K. Khenfer, B. Belkessa, J. Fajoui, B. Cheniti, B. Idir and S. Branchu, Effect of Heat Input on Microstructure, Residual Stress and Corrosion Resistance of UNS 32101 Lean Duplex Stainless Steel Weld Joints, *J. Mater. Eng. Perform.*, 2019, **28**, p 4252–5264
24. A. Turnbull, K. Mingard, J.D. Lord, B. Roebuck, D.R. Tice, K.J. Mottershead, N.D. Fairweather and A.K. Bradbury, Sensitivity of Stress Corrosion Cracking of Stainless Steel to Surface Machining and Grinding Procedure, *Corros. Sci.*, 2011, **53**, p 3398–3415
25. A.K.A. Jawwad, M. Mahdi and N. Alshabatat, The Role of Service-Induced Residual Stresses in Initiating and Propagating Stress Corrosion Cracking (SCC) in a 316 Stainless Steel Pressure-Relief-Valve Nozzle Set, *Eng. Fail. Anal.*, 2019, **105**, p 1229–1251
26. O. Takakuwa and H. Soyama, Effect of Residual Stress on the Corrosion Behavior of Austenitic Stainless Steel, *Adv. Chem. Eng. Sci.*, 2015, **5**, p 62–71
27. Q. Wang, B. Zhang, Y. Ren and K. Yang, A Self-healing Stainless Steel: Role of Nitrogen in Eliminating Detrimental Effect of Cold Working on Pitting Corrosion Resistance, *Corros. Sci.*, 2018, **145**, p 55–66
28. J. Wang and L.F. Zhang, Effects of Cold Deformation on Electrochemical Corrosion Behaviors of 304 Stainless Steel, *Anti-Corros. Methods Mater.*, 2017, **64**, p 252–262
29. U.K. Mudali, P. Shankar, S. Ningshen, R.K. Dayal, H.S. Khatak and B. Raj, On the Pitting Corrosion Resistance of Nitrogen Alloyed Cold Worked Austenitic Stainless Steels, *Corros. Sci.*, 2002, **44**, p 2183–2198
30. N.E. Hakiki, M.F. Montemor, M.G.S. Ferreira and M. Da Cunha Belo, Semiconducting Properties of Thermally Grown Oxide Films on AISI 304 Stainless Steel, *Corros. Sci.*, 2000, **42**, p 687–702
31. A. Latifi, M. Imani, M.T. Khorasani and M.D. Joupari, Plasma Surface Oxidation of 316L Stainless Steel for Improving Adhesion Strength of Silicone Rubber Coating to Metal Substrate, *Appl. Surf. Sci.*, 2014, **320**, p 471–481
32. R.H. Jung, H. Tsuchiya and S. Fujimoto, XPS Characterization of Passive Films Formed on Type 304 Stainless Steel in Humid Atmosphere, *Corros. Sci.*, 2012, **58**, p 62–68
33. Y. Qiu, S. Thomas, D. Fabijanic, A.J. Barlow, H.L. Fraser and N. Birbilis, Microstructural Evolution, Electrochemical and Corrosion Properties of AlxCoCrFeNiTiy High Entropy Alloys, *Mater. Des.*, 2019, **170**, p 170698
34. A.P. Grosvenor, B.A. Kobe, M.C. Biesinger and N.S. McIntyre, Investigation of Multiplet Splitting of Fe 2p XPS Spectra and Bonding in Iron Compounds, *Surf. Interface Anal.*, 2004, **36**, p 1564–1574
35. X. Cheng, Z. Feng, C. Li, C. Doing and X. Li, Investigation of Oxide Film Formation on 316L Stainless Steel in High-Temperature Aqueous Environments, *Electrochim. Acta*, 2011, **56**, p 5860–5865
36. J.L. Rocha, R.S. Pereira, M.C.L. de Oliveira and R.A. Antunes, Investigation on the Relationship Between the Surface Chemistry and the Corrosion Resistance of Electrochemically Nitrided AISI 304 Stainless Steel, *Int. J. Corros.*, 2019, **2019**, p 7023283-1-7023283–12
37. M. Dadfar, M. Salehi, M.A. Golozar, S. Trasatti and M.P. Casaletto, Surface and Corrosion Properties of Modified Passive Layer on 304 Stainless Steel as Bipolar Plates for PEMFCs, *Int. J. Hydrogen Energy*, 2017, **42**, p 25869–25876
38. T. Sömmez, M.F. Jadidi, K. Kazmanli, Ö. Birer and M. Ürgen, Role of Different Plasma Gases on the Surface Chemistry and Wettability of RF Plasma Treated Stainless Steel, *Vacuum*, 2016, **129**, p 63–73
39. A. Latifi, M. Imani, M.T. Khorasani and M.D. Joupari, Electrochemical and Chemical Methods for Improving Surface Characteristics of 316L Stainless Steel for Biomedical Applications, *Surf. Coat. Technol.*, 2013, **221**, p 1–12
40. K. Rokosz, T. Hryniewicz, S. Raaen and J. Valicek, SEM/EDX, XPS, Corrosion and Surface Roughness Characterization of AISI 316L SS After Electrochemical Treatment in Concentrated HNO_3, *Teh. Vjesn.*, 2015, **22**, p 125–131
41. R. Jiang, Y. Wang, X. Wen, C. Chen and J. Zhao, Effect of Time on the Characteristics of Passive Film Formed on Stainless Steel, *Appl. Surf. Sci.*, 2017, **412**, p 214–222
42. Y. Li, Y. He, J. Qiu, J. Zhao, Q. Ye, Y. Zhu and J. Mao, Enhancement of Pitting Corrosion Resistance of Austenitic Stainless Steel Through Deposition of Amorphous/Nanocrystalline Oxy-Nitrided Phases by Active Screen Plasma, *Mater. Res.*, 2018, **21**, p 2017697-1-20170697–10
43. Z. Wang, Z.-Q. Zhou, L. Zhang, J.-Y. Hu, Z.-R. Zhang and M.-X. Lu, Effect of pH on the Electrochemical Behaviour and Passive Film Composition of 316L Stainless Steel, *Acta Metall. Sin. (Engl. Lett.)*, 2019, **32**, p 585–598
44. E. Hamada, K. Yamada, M. Nagoshi, N. Makiishi, K. Sato, T. Ishii, K. Fukuda, S. Ishikawa and T. Ujiro, Direct Imaging of Native Passive Film on Stainless Steel by Aberration Corrected STEM, *Corros. Sci.*, 2010, **52**, p 3851–3854
45. A. Kocijan, C. Donik and M. Jenko, Electrochemical and XPS Studies of the Passive Film Formed on Stainless Steels in Borate Buffer and Chloride Solutions, *Corros. Sci.*, 2007, **49**, p 2083–2098
46. L. Franta, J. Fojt, L. Joska, J. Kronek, L. Cvrcek, J. Vyskocil and Z. Cejka, Hinge-Type Knee Prosthesis Wear Tests with a Mechanical Load and Corrosion Properties Monitoring, *Tribol. Int.*, 2013, **63**, p 61–65
47. T. Hryniewicz, K. Rokosz and M. Filippi, Biomaterial Studies on AISI 316L Stainless Steel After Magnetoelectropolishing, *Materials*, 2009, **2**, p 129–145
48. Y. Yang, Q. Wang, J. Li, L. Tan and K. Yang, Enhancing General Corrosion Resistance of Biomedical High Nitrogen Nickel-Free Stainless Steel by Water Treatment, *Mater. Lett.*, 2019, **251**, p 196–200
49. K. Engvall, J. Pan, A. Kotarba and M. Cies, Silane-Parylene Coating for Improving Corrosion Resistance of Stainless Steel 316L Implant Material, *Corros. Sci.*, 2011, **53**, p 296–301
50. E.M. Sherif, A Comparative Study on the Electrochemical Corrosion Behavior of Iron and X-65 steel in 4.0 wt.% Sodium Chloride Solution After Different Exposure Intervals, *Molecules*, 2014, **19**, p 9962–9974
51. A.S. Hamdy, E. El-Shenawy and T. El-Bitar, Electrochemical Impedance Spectroscopy Study of the Corrosion Behavior of Some Niobium Bearing Stainless Steels in 35% NaCl, *Int. J. Electrochem. Sci.*, 2006, **1**, p 171–180
52. S. Ningshen, M. Sakairi, K. Suzuki and S. Ukai, The Corrosion Resistance and Passive Film Compositions of 12%Cr and 15%Cr Oxide Dispersion Strengthened Steels in Nitric Acid Media, *Corros. Sci.*, 2014, **78**, p 322–334
53. Y. Zhang, H. Luo, Q. Zhong, H. Yu and J. Lv, Characterization of Passive Films Formed on as-received and Sensitized AISI 304 Stainless Steel, *Chin. J. Mech. Eng.*, 2019, **32**, p 27-1-27–12
54. M. Pontinha, S. Faty, M.G. Walls, M.G.S. Ferreira and M. Da Cunha Belo, Electronic Structure of Anodic Oxide Films Formed on Cobalt by Cyclic Voltammetry, *Corros. Sci.*, 2006, **48**, p 2971–2986
55. J. Lv and H. Luo, Comparison of Corrosion Properties of Passive Films Formed on Phase Reversion Induced Nano/Ultrafine-Grained 321 Stainless Steel, *Appl. Surf. Sci.*, 2013, **280**, p 124–131
56. X. Liu and G.S. Frankel, Effects of Compressive Stress on Localized Corrosion in AA2024-T3, *Corros. Sci.*, 2006, **48**, p 3309–3329
57. P. Peyre, X. Scherpereel, L. Berthe, C. Carboni, R. Fabbro, G. Béraner and C. Lemaitre, Surface Modifications Induced in 316L Steel by Laser Peening and Shot-Peening. Influence on Pitting Corrosion Resistance, *Mater. Sci. Eng. A*, 2000, **280**, p 294–302
58. U.K. Mudali, P. Shankar, S. Ningshen, R.K. Daval, H.S. Khatak and B. Raj, On the Pitting Corrosion Resistance of Nitrogen Alloyed Cold Worked Austenitic Stainless Steels, *Corros. Sci.*, 2002, **44**, p 2183–2198
59. V. Vignal, C. Valot, R. Oltra, M. Verneau and L. Coudreuse, Analogy Between the Effects of a Mechanical and Chemical Perturbation on the Conductivity of Passive Films, *Corros. Sci.*, 2002, **44**, p 1477–1496
60. S. Mischler, A. Vogel, H.J. Mathieu and D. Landolt, The Chemical Composition of the Passive Film on Fe-24Cr and Fe-24Cr-11Mo Studied by AES, XPS and SIMS, *Corros. Sci.*, 1991, **32**, p 925–944
61. S. He and D. Jiang, Electrochemical Behavior and Properties of Passive Films on 304 Stainless Steel Under High Temperature and Stress Conditions, *Int. J. Electrochem. Sci.*, 2018, **13**, p 5832–5849
62. Z. Ai, W. Sun, J. Jiang, D. Song, H. Ma, J. Zhang and D. Wang, Passivation Characteristics of Alloy Corrosion-Resistant Steel Cr10Mo1 in Simulating Concrete Pore Solutions: Combination Effects of pH and Chloride, *Materials*, 2016, **9**, p 749-1-749–17
63. D.D. Macdonald, The Point Defect Model for the Passive State, *J. Electrochem. Soc.*, 1992, **139**, p 3434–3449
64. X. Zhang, J. Zhao, T. Si, M.B. Shalzad, C. Yang and K. Yang, Dissolution and Repair of Passive Film on Cu-Bearing 304L Stainless Steels Immersed in H_2SO_4 Solution, *J. Mater. Sci. Technol.*, 2018, **34**, p 2149–2159
65. M. Liu, X. Cheng, X. Li, Y. Pan and J. Li, Effect of Cr on the Passive Film Formation Mechanism of Steel Rebar in Saturated Calcium Hydroxide Solution, *Appl. Surf. Sci.*, 2016, **389**, p 1182–1191

66. J. Amri, T. Souier, B. Malki and B. Baroux, Effect of the Final Annealing of Cold Rolled Stainless Steels Sheets on the Electronic Properties and Pit Nucleation Resistance of Passive Films, *Corros. Sci.*, 2008, **50**, p 431–435
67. Z. Feng, X. Cheng, C. Dong, L. Xu and X. Li, Passivity of 316L Stainless Steel in Borate Buffer Solution Studied by Mott-Schottky Analysis, Atomic Absorption Spectrometry and X-ray Photoelectron Spectroscopy, *Corros. Sci.*, 2010, **52**, p 3646–3653